ARMY RESEARCH LABORATORY

Model of Predictive Control of a Direct-Fire Projectile Equipped With Canards

by Douglas Ollerenshaw and Mark Costello

ARL-CR-558 **March 2005**

prepared by

The Department of Mechanical Engineering
Oregon State University
Corvallis, OR 97331

under contract
W911QX-04-P0270

NOTICES

Disclaimers

The findings in this report are not to be construed as an official Department of the Army position unless so designated by other authorized documents.

Citation of manufacturer's or trade names does not constitute an official endorsement or approval of the use thereof.

Destroy this report when it is no longer needed. Do not return it to the originator.

Army Research Laboratory
Aberdeen Proving Ground, MD 21005-5066

ARL-CR-558 **March 2005**

Model of Predictive Control of a Direct-Fire Projectile Equipped With Canards

Douglas Ollerenshaw and Mark Costello
Weapons and Materials Research Directorate, ARL

prepared by

The Department of Mechanical Engineering
Oregon State University
Corvallis, OR 97331

under contract
W911QX-04-P0270

REPORT DOCUMENTATION PAGE

Form Approved
OMB No. 0704-0188

1. REPORT DATE *(DD-MM-YYYY)*	2. REPORT TYPE	3. DATES COVERED (From - To)
March 2005	Final	January 2004–September 2004

4. TITLE AND SUBTITLE
Model of Predictive Control of a Direct-Fire Projectile Equipped With Canards

5a. CONTRACT NUMBER
W911QX-04-P0270

5b. GRANT NUMBER

5c. PROGRAM ELEMENT NUMBER

6. AUTHOR(S)
Douglas Ollerenshaw* and Mark Costello†

5d. PROJECT NUMBER
AH80

5e. TASK NUMBER

5f. WORK UNIT NUMBER

7. PERFORMING ORGANIZATION NAME(S) AND ADDRESS(ES)
Department of Mechanical Engineering
Oregon State University
Corvallis, OR 97331

8. PERFORMING ORGANIZATION REPORT NUMBER

9. SPONSORING/MONITORING AGENCY NAME(S) AND ADDRESS(ES)
U.S. Army Research Laboratory
ATTN: AMSRD-ARL-WM-BC
Aberdeen Proving Ground, MD 21005-5066

10. SPONSOR/MONITOR'S ACRONYM(S)

11. SPONSOR/MONITOR'S REPORT NUMBER(S)
ARL-CR-558

12. DISTRIBUTION/AVAILABILITY STATEMENT
Approved for public release; distribution is unlimited.

13. SUPPLEMENTARY NOTES
* Graduate research assistant
†Associate professor, member ASME

14. ABSTRACT

Launch uncertainties in uncontrolled direct-fire projectiles can lead to significant impact point dispersion, even at relatively short range. A model predictive control scheme for direct-fire projectiles is investigated to reduce impact point dispersion. The control law depends on projectile linear theory to create an approximate linear model of the projectile and quickly predict states into the future. Control inputs are based on minimization of the error between predicted projectile states and a desired trajectory leading to the target. Through simulation, the control law is shown to work well in reducing projectile impact point dispersion. Parametric trade studies on an example projectile configuration are reported that detail the effect of prediction horizon length, gain settings, model update interval, and model step size.

15. SUBJECT TERMS
guided munition, direct fire, canard control

16. SECURITY CLASSIFICATION OF:			17. LIMITATION OF ABSTRACT	18. NUMBER OF PAGES	19a. NAME OF RESPONSIBLE PERSON
a. REPORT	b. ABSTRACT	c. THIS PAGE			Peter Plostins
UNCLASSIFIED	UNCLASSIFIED	UNCLASSIFIED	UL	40	19b. TELEPHONE NUMBER (*Include area code*) 410-278-8878

Standard Form 298 (Rev. 8/98)
Prescribed by ANSI Std. Z39.18

Contents

List of Figures

List of Tables

1. Introduction

Direct-fire projectiles are fired by line-of-sight aiming and are fired from ground-based platforms, helicopters, and fixed wing aircraft. A number of conditions can cause rounds to miss an intended target. These conditions include manufacturing inaccuracies of the gun tube, propellant, or projectile, along with variable atmospheric conditions, firing platform motion, and aiming errors. With the advent of low-cost, small, rugged, microelectromechanical systems, dramatic reduction of dispersion for direct-fire projectiles equipped with a relatively inexpensive flight control system is possible. One design concept consists of a set of controllable canards located near the nose of the projectile. This report develops a unique flight control law tailored to the control of smart projectiles through the application of model predictive control and projectile linear theory.

In model predictive control, a dynamic model of the plant is used to project the state into the future and subsequently use the estimated future state to determine control action. It has been found to be a practical and increasingly employed control technique (*1*). Currently, model predictive control is being applied to a wide variety of problems, spanning many different industries. Mei et al. (*2*) studied vibration reduction of a tall building experiencing wind excitation using model predictive control and linear quadratic guassian control strategies. They found that the model predictive control scheme performed well and was robust to uncertainty in building stiffness. Tsai and Huang (*3*) used a model reference adaptive predictive controller for a variable-frequency oil-cooling machine used in concert with dynamically complex machine tools. Kvaternik et al. (*4*) developed a generalized predictive controller for tilt rotor aeroelastic stability augmentation in airplane mode of flight. Using the model predictive control strategy, significant increases in damping of aircraft body vibration modes were achieved in a wind tunnel test. Slegers and Costello (*5*) applied model predictive control to a parafoil for autonomous delivery of a payload in battlefield conditions. Burchett and Costello (*6*) used a simplified form of model predictive control applied to a projectile with lateral pulsejets. Their strategy was to use projectile linear theory to map the projected impact point in the vertical target plane and base control action on projected miss distance and direction. The key difference between their strategy and that detailed here is that the control strategy employed by Burchett and Costello calculated errors only in the target plane, while the control strategy used here considers error along the length of the trajectory. In addition, the pulsejet control scheme used by Burchett and Costello is inherently discontinuous and can only be applied at a discrete number of points. Canard control, as applied in this report, is continuous and is applied for the full flight duration.

Any model predictive control scheme is dependent upon the accuracy of the underlying dynamic model representing the plant. Under most flight conditions, the equations of motion for a projectile in atmospheric flight can be adequately represented by a six-degree-of-freedom rigid

body model with externally-applied aerodynamic forces and moments. The resulting differential equations have been shown to provide an accurate representation of projectile flight characteristics (*7*), though their inherent nonlinearity prevents direct use in model-predictive control applications. However, a series of manipulations and simplifications of the equations of motion allow closed form solution of the projectile trajectory under restricted flight conditions. The simplified dynamic equations and their resulting solutions have become known as projectile linear theory. Projectile linear theory has been extended by various authors to handle more sophisticated aerodynamic models (*8*), asymmetric mass properties (*9*), fluid payloads (*10*, *11*), moving internal parts (*12*, *13*), dual spin projectiles (*14*, *15*), ascending flight (*16*), and lateral force impulses (*17–20*). Aerodynamic range reduction software used in spark range facilities utilizes projectile linear theory in estimation of aerodynamic coefficients.

The reported work employs model predictive control and projectile linear theory for control of a direct-fire projectile. The basic projectile configuration under consideration is fin stabilized, and the fins are slightly canted to provide moderate roll rates during flight. A set of controllable canards located near the nose of the projectile are used as the control mechanism. The canards can be directed to provide swerve forces and pitch and yaw moments to the projectile. The control law uses an approximate closed form solution of projectile motion to predict the states of the projectile over a set distance known as the prediction horizon. Current and future control actions are determined based on minimizing the estimated error of future states. It is assumed that sensor feedback is provided by an onboard inertial measurement unit (IMU). Simulation results to establish the utility of the new model predictive flight control system design methodology are generated for an exemplar projectile. Parametric trade studies are conducted that consider the effect of the cost function weighting matrices, prediction horizon length, state estimation step size, and the model update interval on impact point dispersion.

2. Projectile Dynamic Model

The nonlinear trajectory simulation used in this study is a standard six-degree-of-freedom model typically used in flight dynamic modeling of projectiles. A schematic of the projectile configuration is shown in figures 1 and 2. The six degrees of freedom are the three inertial components of the position vector from an inertial frame to the projectile mass center and the three standard Euler orientation angles.

The equations of motion are provided in equations 1–4 (*21–23*).

$$\begin{Bmatrix} \dot{x} \\ \dot{y} \\ \dot{z} \end{Bmatrix} = \begin{bmatrix} c_\theta c_\psi & s_\phi s_\theta c_\psi - c_\phi s_\psi & c_\phi s_\theta c_\psi + s_\phi s_\psi \\ c_\theta s_\psi & s_\phi s_\theta s_\psi + c_\phi c_\psi & c_\phi s_\theta s_\psi - s_\phi c_\psi \\ -s_\theta & s_\phi c_\theta & c_\phi c_\theta \end{bmatrix} \begin{Bmatrix} u \\ v \\ w \end{Bmatrix}. \quad (1)$$

$$\begin{Bmatrix} \dot{\phi} \\ \dot{\theta} \\ \dot{\psi} \end{Bmatrix} = \begin{bmatrix} 1 & s_\phi t_\theta & c_\phi t_\theta \\ 0 & c_\phi & -s_\phi \\ 0 & s_\phi / c_\theta & c_\phi / c_\theta \end{bmatrix} \begin{Bmatrix} p \\ q \\ r \end{Bmatrix}. \tag{2}$$

$$\begin{Bmatrix} \dot{u} \\ \dot{v} \\ \dot{w} \end{Bmatrix} = \begin{Bmatrix} X/m \\ Y/m \\ Z/m \end{Bmatrix} - \begin{bmatrix} 0 & -r & q \\ r & 0 & -p \\ -q & p & 0 \end{bmatrix} \begin{Bmatrix} u \\ v \\ w \end{Bmatrix}. \tag{3}$$

$$\begin{Bmatrix} \dot{p} \\ \dot{q} \\ \dot{r} \end{Bmatrix} = [I]^{-1} \left[\begin{Bmatrix} L \\ M \\ N \end{Bmatrix} - \begin{bmatrix} 0 & -r & q \\ r & 0 & -p \\ -q & p & 0 \end{bmatrix} [I] \begin{Bmatrix} p \\ q \\ r \end{Bmatrix} \right]. \tag{4}$$

In equations 1 and 2, the standard shorthand notation for trigonometric functions is used: $\sin(\alpha) \equiv s_\alpha$, $\cos(\alpha) \equiv c_\alpha$, and $\tan(\alpha) \equiv t_\alpha$. The forces in equation 3 contain contributions from weight (W), body aerodynamics (A), and the control canards (C).

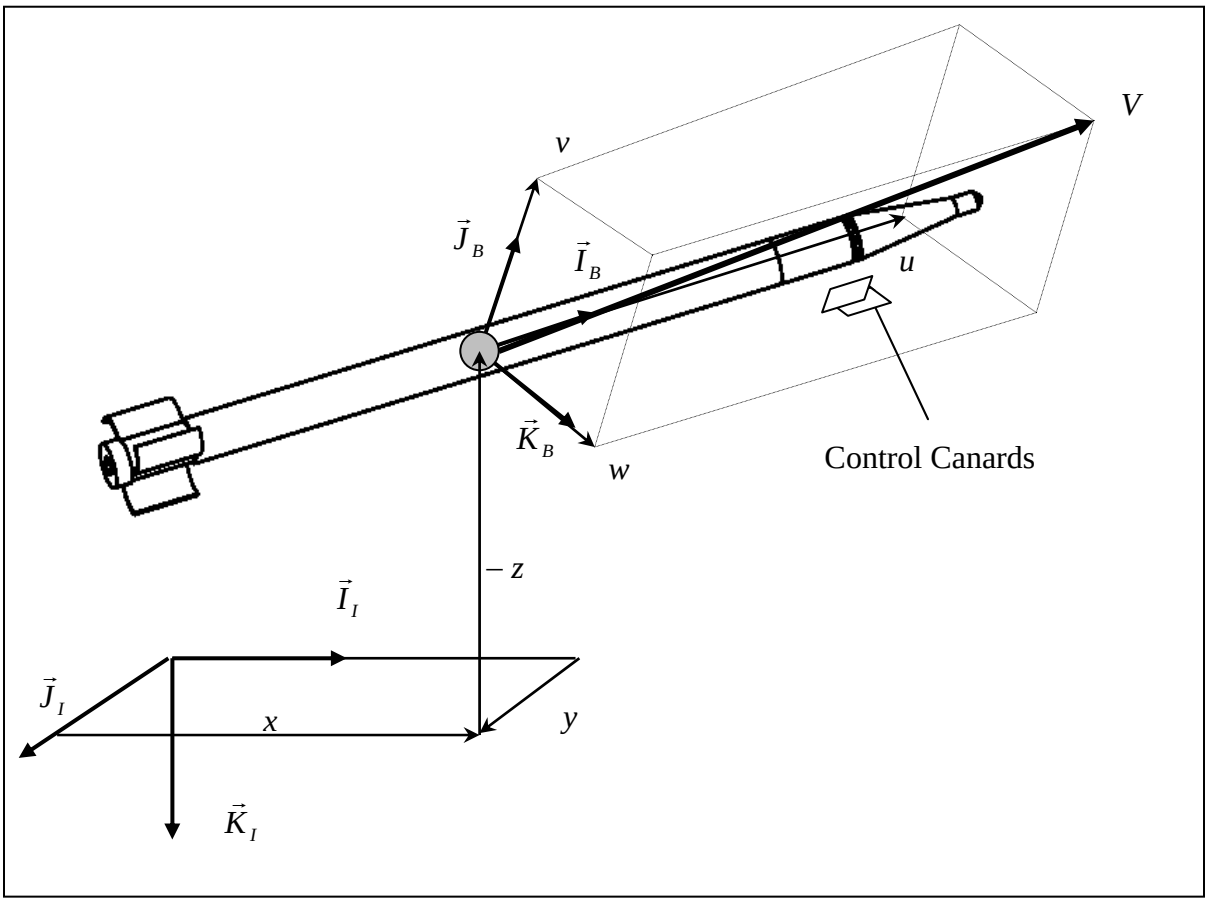

Figure 1. Schematic of the position coordinates of a direct-fire projectile.

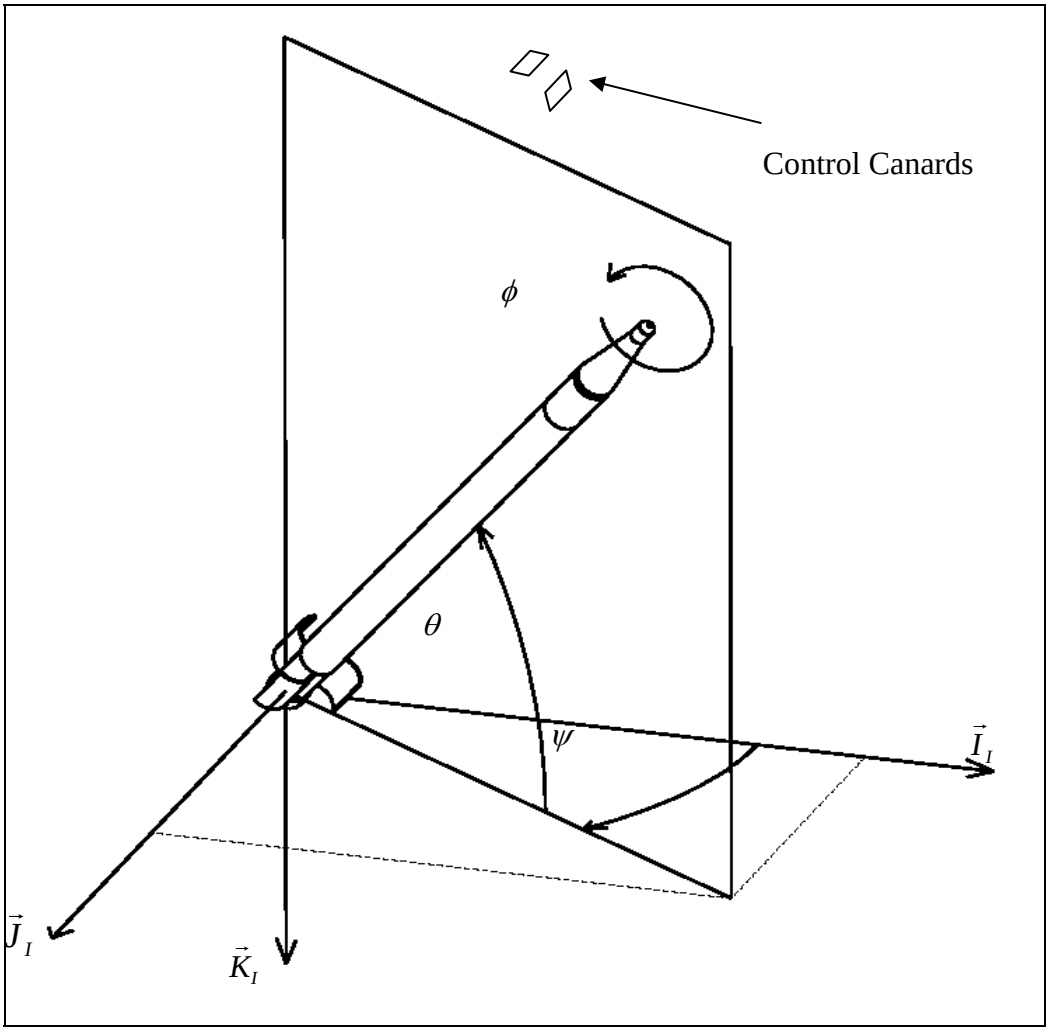

Figure 2. Schematic of the attitude coordinates of a direct-fire projectile.

$$\begin{Bmatrix} X \\ Y \\ Z \end{Bmatrix} = \begin{Bmatrix} X_W \\ Y_W \\ Z_W \end{Bmatrix} + \begin{Bmatrix} X_A \\ Y_A \\ Z_A \end{Bmatrix} + \begin{Bmatrix} X_C \\ Y_C \\ Z_C \end{Bmatrix}. \tag{5}$$

The dynamic equations are expressed in a body-fixed reference frame, thus all forces acting on the body are expressed in the projectile reference frame. The weight force is shown in equation 6:

$$\begin{Bmatrix} X_W \\ Y_W \\ Z_W \end{Bmatrix} = mg \begin{Bmatrix} -s_\theta \\ s_\phi c_\theta \\ c_\phi c_\theta \end{Bmatrix}, \tag{6}$$

while the aerodynamic force acting at the center of pressure of the projectile is given by equation 7:

$$\begin{Bmatrix} X_A \\ Y_A \\ Z_A \end{Bmatrix} = -\frac{\pi}{8}\rho V^2 D^2 \begin{Bmatrix} C_{X0} + C_{X2}(v^2 + w^2)/V^2 \\ C_{NA} v \ /V \\ C_{NA} w \ /V \end{Bmatrix}. \tag{7}$$

The control forces are the aerodynamic drag forces created by the control canards in the directions perpendicular to the axis of symmetry of the projectile:

$$\begin{Bmatrix} X_C \\ Y_C \\ Z_C \end{Bmatrix} = -\frac{\pi}{8}\rho V^2 D^2 \begin{Bmatrix} 0 \\ C_{Y0} \\ C_{Z0} \end{Bmatrix}. \tag{8}$$

The applied moments about the projectile mass center contain contributions from steady aerodynamics (SA), unsteady aerodynamics (UA), and the control canards (C):

$$\begin{Bmatrix} L \\ M \\ N \end{Bmatrix} = \begin{Bmatrix} L_{SA} \\ M_{SA} \\ N_{SA} \end{Bmatrix} + \begin{Bmatrix} L_{UA} \\ M_{UA} \\ N_{UA} \end{Bmatrix} + \begin{Bmatrix} L_C \\ M_C \\ N_C \end{Bmatrix}. \tag{9}$$

The moment components due to steady aerodynamic forces and control canard forces are computed with a cross product between the distance vector from the mass center to the location of the specific force and the force itself. The unsteady body aerodynamic moment provides a damping source for projectile angular motion and is given by equation 10:

$$\begin{Bmatrix} L_{UA} \\ M_{UA} \\ N_{UA} \end{Bmatrix} = \frac{\pi}{8}\rho V^2 D^3 \begin{Bmatrix} C_{DD} + \dfrac{pDC_{LP}}{2V} \\ \dfrac{qDC_{MQ}}{2V} \\ \dfrac{rDC_{MQ}}{2V} \end{Bmatrix}. \tag{10}$$

The mass, mass center location, and inertial properties of the projectile are all assumed to be constant throughout the duration of the flight. The center of pressure location and all aerodynamic coefficients ($C_{X0}, C_{YPA}, C_{NA}, C_{DD}, C_{LP}, C_{MQ}$) depend on local Mach number and are computed during simulation using linear interpolation.

The dynamic equations given by equations 1–4 are numerically integrated forward in time using a 4th order, fixed step Runge-Kutta algorithm. Costello and Anderson (*7*) present correlation of this dynamic model against range data for a fin-stabilized projectile.

3. Projectile Linear Theory Trajectory Solution

The six-degree-of-freedom rigid body projectile model shown earlier consists of 12 highly nonlinear differential equations for which a closed form solution has not been directly found. Significant work has been performed to simplify the equations of motion such that an accurate analytical solution can be determined. In order to arrive at a set of analytically solvable ordinary linear differential equations, the following assumptions and simplifications are made:

1. Rather than employing a reference frame fixed to the projectile body, projectile linear theory uses an intermediate reference frame which is aligned with the projectile axis of symmetry but does not roll. Lateral translational and rotational velocity components described in this frame, known as the no-roll frame or the fixed plane frame, are denoted with a ~ superscript. Components of the linear and angular body velocities in the fixed plane frame are computed from body frame components of the same vector through a single axis rotation transformation. For example, the body frame components of the projectile mass center velocity are transformed to the fixed plane by

$$\begin{Bmatrix} \tilde{u} \\ \tilde{v} \\ \tilde{w} \end{Bmatrix} = \begin{bmatrix} 1 & 0 & 0 \\ 0 & c_\phi & -s_\phi \\ 0 & s_\phi & c_\phi \end{bmatrix} \begin{Bmatrix} u \\ v \\ w \end{Bmatrix}. \tag{11}$$

2. A change of variables is made from the velocity along the projectile axis of symmetry, u, to the total velocity, V. Equations 12 and 13 relate V and u and their derivatives:

$$V = \sqrt{u^2 + v^2 + w^2} = \sqrt{u^2 + \tilde{v}^2 + \tilde{w}^2}\ ; \tag{12}$$

$$\dot{V} = \frac{u\dot{u} + v\dot{v} + w\dot{w}}{V} = \frac{u\dot{u} + \tilde{v}\dot{\tilde{v}} + \tilde{w}\dot{\tilde{w}}}{V}\ . \tag{13}$$

3. Dimensionless arc length, s, is used as the independent variable instead of time, t. Equation 14 defines dimensionless arc length:

$$s = \frac{1}{D}\int_0^t V dt\ . \tag{14}$$

Equations 15 and 16 relate time and arc length derivatives of a dummy variable ζ. Dotted terms refer to time derivatives and primed terms denote arc length derivatives:

$$\dot{\zeta} = \left(\frac{V}{D}\right)\zeta'\ ; \tag{15}$$

$$\ddot{\zeta} = \left(\frac{V}{D}\right)^2 \left(\zeta'' + \frac{\zeta' V'}{V}\right). \tag{16}$$

4. Euler pitch and yaw angles are assumed to be small so that

$$\begin{aligned} \sin(\theta) \approx \theta \quad \cos(\theta) \approx 1 \\ \sin(\psi) \approx \psi \quad \cos(\psi) \approx 1. \end{aligned} \tag{17}$$

5. Aerodynamic angles of attack are small so that

$$\alpha \approx \frac{w}{V} \quad \beta \approx \frac{v}{V}. \tag{18}$$

6. The projectile is mass-balanced such that the center of gravity lies in the rotational axis of symmetry:

$$\begin{aligned} I_{xy} = I_{xz} = I_{yz} = 0 \\ I_R = I_{xx} \\ I_P = I_{yy} = I_{zz} \quad . \end{aligned} \tag{19}$$

7. Quantities V and ϕ are large compared to $\theta, \psi, v, w, q,$ and r such that products of small quantities and their derivatives are negligible.

A more detailed discussion of the development of projectile linear theory is provided by McCoy (*21*). Application of the above stated assumptions leads to a set of coupled linear differential equations, with the exception that the total velocity, V, the roll rate, p, and the pitch angle, θ, appear in nonlinear fashion in many of the equations. To remedy this, the assumption is made that V changes slowly with respect to the other variables and is thus considered to be constant, $V = V_0$, when it appears as a coefficient in all dynamic equations except its own. In addition, the roll rate and pitch angle are held constant, $p = p_0$ and $\theta = \theta_0$, only when they appear in nonlinear fashion. The equation for the total velocity is shown as equation 20:

$$V' = \frac{-\pi \rho D^3 C_{X0}}{8m} V - \frac{DgS_{\theta_0}}{V}. \tag{20}$$

The remaining 11 equations can be written as

$$\begin{Bmatrix} \tilde{v}' \\ \tilde{w}' \\ \tilde{q}' \\ \tilde{r}' \\ x' \\ y' \\ z' \\ \phi' \\ \theta' \\ \psi' \\ p' \end{Bmatrix} = \begin{bmatrix} -A & 0 & 0 & -D & 0 & 0 & 0 & 0 & 0 & 0 & 0 \\ 0 & -A & D & 0 & 0 & 0 & 0 & 0 & 0 & 0 & 0 \\ B/D & C/D & H & -F & 0 & 0 & 0 & 0 & 0 & 0 & 0 \\ -C/D & B/D & F & H & 0 & 0 & 0 & 0 & 0 & 0 & 0 \\ 0 & 0 & 0 & 0 & 0 & 0 & 0 & 0 & 0 & 0 & 0 \\ D/V_0 & 0 & 0 & 0 & 0 & 0 & 0 & 0 & 0 & D & 0 \\ 0 & D/V_0 & 0 & 0 & 0 & 0 & 0 & 0 & -D & 0 & 0 \\ 0 & 0 & 0 & 0 & 0 & 0 & 0 & 0 & 0 & 0 & D/V_0 \\ 0 & 0 & D/V_0 & 0 & 0 & 0 & 0 & 0 & 0 & 0 & 0 \\ 0 & 0 & 0 & D/V_0 & 0 & 0 & 0 & 0 & 0 & 0 & 0 \\ 0 & 0 & 0 & 0 & 0 & 0 & 0 & 0 & 0 & 0 & K_c \end{bmatrix} \begin{Bmatrix} \tilde{v} \\ \tilde{w} \\ \tilde{q} \\ \tilde{r} \\ x \\ y \\ z \\ \phi \\ \theta \\ \psi \\ p \end{Bmatrix} + \begin{Bmatrix} V_F \\ W_F \\ Q_F \\ R_F \\ D \\ 0 \\ 0 \\ 0 \\ 0 \\ 0 \\ P_F \end{Bmatrix}, \tag{21}$$

where

$$A = \frac{\pi\rho D^3 C_{NA}}{8m}, \tag{22}$$

$$B = \frac{\pi\rho D^5 C_{YPA} p_0 \Delta SL_m}{16 I_P V_0}, \tag{23}$$

$$C = \frac{\pi\rho D^4 C_{NA} \Delta SL}{8 I_P}, \tag{24}$$

$$F = \frac{I_R D p_0}{I_P V_0}, \tag{25}$$

$$H = \frac{\pi\rho D^5 C_{MQ}}{16 I_P}, \tag{26}$$

$$K_C = \frac{\pi\rho D^5 C_{LP}}{16 I_R}, \tag{27}$$

$$V_F = \frac{\pi\rho D^3}{8m}\left(C_{NA}\tilde{v}_* - V_0 C_{Y0}\right), \tag{28}$$

$$W_F = \frac{gDC_{\theta_0}}{V_0} + \frac{\pi\rho D^3}{8m}\left(C_{NA}\tilde{w}_* - V_0 C_{Z0}\right), \tag{29}$$

$$Q_F = \frac{\pi\rho D^3}{8 I_P}\left(-\tilde{w}_* C_{NA}\Delta SL - \frac{DC_{YPA} p_0 \Delta SL_m \tilde{v}_*}{2V_0} + V_0 C_{Z0}\Delta SL_C\right), \tag{30}$$

$$R_F = \frac{\pi\rho D^3}{8I_P}\left(-\tilde{v}_* C_{NA}\Delta SL - \frac{DC_{YPA}p_0\Delta SL_m\tilde{w}_*}{2V_0} - V_0 C_{Y0}\Delta SL_C\right), \text{ and} \tag{31}$$

$$P_F = \frac{\pi\rho V_0 D^4 C_{DD}}{8I_R}. \tag{32}$$

Closed form solutions to the above equations can be found, though the results are omitted here. A more detailed treatment of the solutions to the projectile linear theory equations can be found in reference (*23*).

The variables C_{Y0} and C_{Z0} are aerodynamic trim forces perpendicular to the projectile axis of symmetry, which are created by movement of the control canards and are treated directly as control inputs.

In reality, the total velocity, V, does not remain constant for the duration of the flight; therefore, the total velocity must be periodically measured throughout the trajectory and updated in the remaining equations. The center of pressure location and the aerodynamic coefficients ($C_{X0}, C_{YPA}, C_{NA}, C_{DD}, C_{LP}, C_{MQ}$), which all depend on local Mach number, must also be recomputed each time V is updated. The effect of the length of the update interval on the accuracy of the model was studied by Burchett et al. (*19*).

4. Model-Predictive Flight Control System

The model-predictive controller uses the linearized model of the system to propagate the states forward in time over an interval known as the prediction horizon $\left(H_p\right)$ (*24*). Control action is based on comparison of the predicted states and a predetermined desired trajectory over the prediction horizon. As the prediction step is marched forward, so too is the prediction horizon—a process referred to as the "receding horizon principle." The control action at each step is determined by minimizing a quadratic cost function, defined as

$$J = \left(W - \tilde{Y}\right)^T Q\left(W - \tilde{Y}\right) + U^T RU. \tag{33}$$

The matrix W contains the desired system outputs, w, over the length of the prediction horizon. The desired system outputs, w, at each prediction step consists of the desired x, y, and z coordinates at that time instant. These values need to be loaded into the onboard computer prior to projectile launch.

$$W = \begin{Bmatrix} w_{k+1} \\ w_{k+2} \\ \vdots \\ w_{k+Hp} \end{Bmatrix} \quad w_{k+i} = \begin{Bmatrix} x_{k+i} \\ y_{k+i} \\ z_{k+i} \end{Bmatrix}. \tag{34}$$

The matrix $\tilde{Y}$ contains the predicted system outputs, $\tilde{y}$, and the matrix U contains the calculated system inputs, u, as follows:

$$\tilde{Y} = \begin{Bmatrix} \tilde{y}_{k+1} \\ \tilde{y}_{k+2} \\ \vdots \\ \tilde{y}_{k+Hp} \end{Bmatrix} \quad U = \begin{Bmatrix} u_k \\ u_{k+1} \\ \vdots \\ u_{k+Hp-1} \end{Bmatrix}. \tag{35}$$

Q and R are diagonal, positive semidefinite weighting matrices.

In order to develop an expression for the predicted system outputs over the prediction horizon, the system is first cast in standard discrete state-space form:

$$\begin{aligned} x_{k+1} &= A(\Delta s)x_k + \mathrm{B}(\Delta s)u_k + \mathrm{F}(\Delta s) \\ y_k &= Cx_k, \end{aligned} \tag{36}$$

where the values within the matrices A, B, and F depend on the arc length step size(Δs). The projectile linear theory expressions shown in the previous section are used to form the state space matrices through a 14-step loop in the control algorithm. In the first step, all the states and controls are set to zero and the solutions are evaluated over one arc length step to determine the values within the constant vector F. In the next step, the first state, $\tilde{u}$, is set equal to one, with the remaining states and controls still equal to zero, and the expressions are reevaluated. By subtracting the values of the constants, F, the coefficients making up the first column of A can be found. This process, consisting of setting a state variable equal to one, evaluating the linear theory solutions, then subtracting the constant values, is repeated for each of the remaining 10 states to fully populate the state matrix A one column at a time. The control matrix, B, is formed in exactly the same manner with all 11 states equal to zero and the controls, C_{Y0} and C_{Z0} alternately set equal to one.

The desired outputs of the system are its center of mass position states (*x*, *y*, and *z*). The matrix C is then simply

$$C = \begin{bmatrix} 0 & 0 & 0 & 0 & 1 & 0 & 0 & 0 & 0 & 0 & 0 \\ 0 & 0 & 0 & 0 & 0 & 1 & 0 & 0 & 0 & 0 & 0 \\ 0 & 0 & 0 & 0 & 0 & 0 & 1 & 0 & 0 & 0 & 0 \end{bmatrix}. \tag{37}$$

A recursive formula can be found for $y_{k+j}, 1 \le j \le H_p$ by substituting the expression for x_{k+j} into the expression for y_{k+j}. The result is

$$y_{k+j} = CA^j x_k + \sum_{i=1}^{j} CA^{j-i} B u_{k+i-1} + \sum_{i=1}^{j} CA^{j-i} F \,, \tag{38}$$

or, in matrix form,

$$\tilde{Y} = K_{CA} x_k + K_{CAB} U + K_{CAF} \,, \tag{39}$$

where

$$K_{CA} = \begin{bmatrix} CA \\ CA^2 \\ CA^3 \\ \vdots \\ CA^{HP} \end{bmatrix}, \tag{40}$$

$$K_{CAB} = \begin{bmatrix} CB & 0 & 0 & \cdots & 0 \\ CAB & CB & 0 & \cdots & \vdots \\ CA^2B & CAB & CB & \cdots & 0 \\ \vdots & \vdots & \vdots & \ddots & 0 \\ CA^{HP-1}B & \cdots & CA^2B & CAB & CB \end{bmatrix}, \text{ and} \tag{41}$$

$$K_{CAF} = \begin{bmatrix} CF \\ CAF + CF \\ CA^2F + CAF + CF \\ \vdots \\ CA^{HP-1}F + \cdots + CAF + CF \end{bmatrix}. \tag{42}$$

The cost function, J, then becomes

$$J = (W - K_{CA} x_k - K_{CAB} U - K_{CAF})^T Q (W - K_{CA} x_k - K_{CAB} U - K_{CAF}) + U^T R U \,. \tag{43}$$

The minimum of the cost function is determined by selecting the control input vector that forces the gradient of the cost function to zero:

$$U = K\left(W - K_{CA} x_k - K_{CAF}\right), \tag{44}$$

where

$$K = \left(K_{CAB}{}^T Q K_{CAB} + R\right)^{-1} K_{CAB}{}^T Q \,. \tag{45}$$

It should be noted that U contains the optimal control inputs over the entire prediction horizon. At each arc length step, k, only u_k is used, which is the first element of U. The first element of U is

$$u_k = K_1\left(W - K_{CA}x_k - K_{CAF}\right), \tag{46}$$

where K_1 consists only of the first M rows of K. Note that M is defined as the number of control inputs which, in this application, is two (C_{Y0} and C_{Z0}).

It is assumed that full-state feedback is available for use in the control law; that is, $x, y, z, \psi, \theta, \phi, u, v, w, p, q,$ and r are sensed or estimated by the IMU. Furthermore, the weapon that fires the projectile provides a desired trajectory leading to the target. At time = 0, the controller is provided with the full state of the projectile. The total velocity, V, is calculated from the projectile mass center velocity states and set to V_0 in the linear model. The linear model is then used to propagate the remaining 11 states forward by Δs. These values are used to populate the A, B, and F matrices, which are sent to the MPC routine. The MPC routine calculates the optimal control sequence over the length of the update interval. When the projectile has covered the length of the first update interval, as well as every subsequent update interval, the controller is provided with full state feedback and the process is repeated. The control sequence calculated by the model predictive controller contains control inputs at increments of Δs. Linear interpolation is applied to determine control inputs between increments of Δs.

It is important to note that the controls resulting from the earlier calculations are expressed in the fixed plane frame, as per assumption number 1 in the linear theory section of this report. To be applied to the canards, the control inputs must be converted to the conventional body fixed reference frame.

Each time the Mach number is updated in the linear model, the matrices A, B, and F are updated as well. This in turn requires updating of the gain matrices. The size of each of these matrices, and hence the computational time required to calculate them, is governed by the length of the prediction horizon. Obviously, frequent updates to the linear model and a long prediction horizon provide greater accuracy in the predictor and more efficient control. These observations are tempered with the need to limit the computational demand placed on the onboard processor.

5. Results

To establish the utility of the model-predictive controller in a projectile application, a 4.5-ft long fin-stabilized projectile is considered. The projectile has a total weight of 22.9748 lb, a center of gravity location of 2.5 ft from the base, and four tail-mounted stabilization fins. The roll and pitch inertia of the body are 0.0057 and 1.35 slug-ft^2, respectively. A set of controllable canards,

which alter the aerodynamic forces and moments, are located 4.25 ft from the base of the projectile.

To model uncertainty in launch conditions, which is a primary cause of dispersion, the initial pitch and yaw rates, pitch and yaw angles, and body velocities are all considered to be normally-distributed random numbers with means and standard deviations that are representative of actual launch uncertainties. The values chosen are shown in table 1.

Table 1. Initial condition uncertainty parameters for dispersion analysis.

Initial Condition	Mean	Standard Deviation
Pitch angle (θ)	0.1 rad	0.01 rad
Yaw angle (ψ)	0.0 rad	0.01 rad
Pitch rate (q)	–0.18 rad/s	2.0 rad/s
Yaw rate (r)	0.0 rad/s	2.0 rad/s
x body velocity (u)	1143.3797 ft/s	15 ft/s
y body velocity (v)	–0.00002502 ft/s	3 ft/s
z body velocity (w)	0.375346 ft/s	3 ft/s

The desired trajectory is chosen as that which the projectile would follow in the absence of uncertainty with initial conditions of x_0, y_0, z_0, ψ_0, ϕ_0, and $r_0 = 0$, $\theta_0 = 0.1$ rad, $u_0 = 1143.38$ ft/s, $v_0 = -2.502\text{x}10^{-5}$ ft/s, $w_0 = 0.375$ ft/s, $p_0 = 51.5$ rad/s, and $q_0 = -0.18$ rad/s. The target location is chosen as $x = 6216.613$ ft, $y = 0.261$ ft, and $z = 0.0$ ft. Figure 3 shows typical dispersion results for 50 sample trajectories with no control applied and initial condition perturbations as described earlier. The circular error probable (CEP) shown in the figure is based on a 50% hit criterion; that is, the CEP is defined as the minimum radius of a circle centered at the mean impact point and containing at least 50% of the shot impact points. With no control applied, the CEP is 106 ft. For reference, a second CEP is shown, which, instead of being centered at the mean impact point, is instead centered at the target location. A 50% hit criterion is still used. The second CEP has a radius of 113.5 ft.

Figure 4 shows the dispersion results with model-predictive control applied. The prediction horizon, H_p, is chosen as 50. The error weighting matrix, Q, is chosen to be a function of range as follows:

$$Q = q\begin{bmatrix} \left(\frac{s_k}{1000}\right)^2 & 0 & 0 & 0 \\ 0 & \left(\frac{s_{k+1}}{1000}\right)^2 & 0 & 0 \\ 0 & 0 & \ddots & \vdots \\ 0 & 0 & \cdots & \left(\frac{s_{k+H_p-1}}{1000}\right)^2 \end{bmatrix}, \tag{47}$$

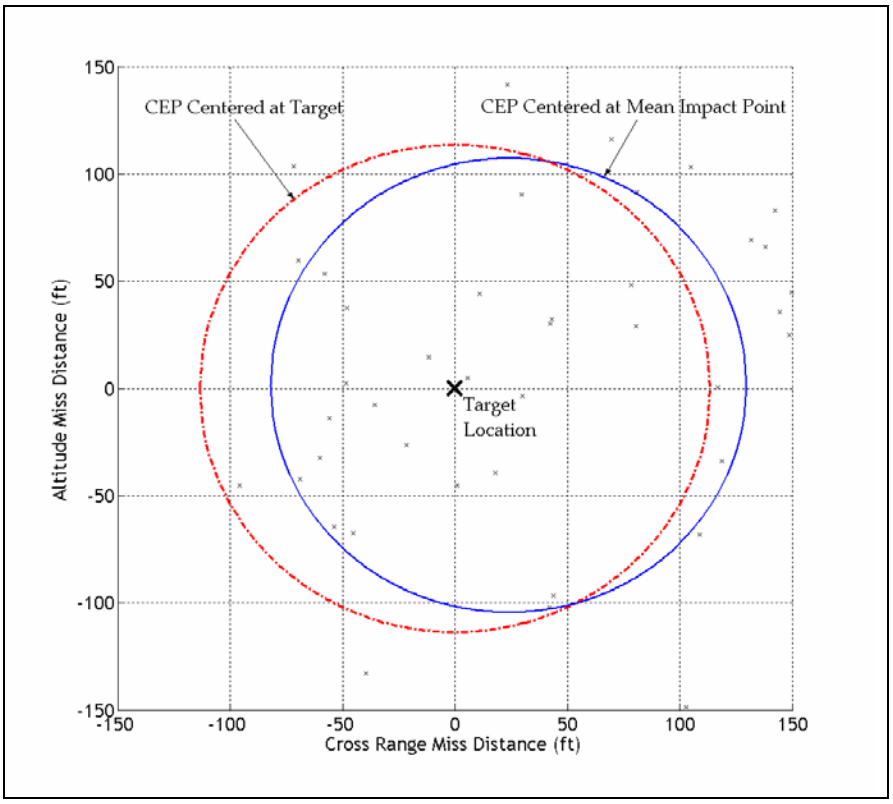

Figure 3. Uncontrolled dispersion (CEP = 113.5 ft centered at mean impact point).

in which q is chosen, in this case, to be 0.5. By defining Q in this manner, the error weighting is increased quadratically as the projectile flies downrange. This prevents the tendency for the controller to attempt to force the projectile onto the desired trajectory immediately after launch, leading to a large initial control input followed by subsequent control inputs of nearly zero. In addition, the control weighting matrix, R, is defined to be

$$R = r\begin{bmatrix} H_p & 0 & 0 & 0 & 0 \\ 0 & H_p - 1 & 0 & 0 & 0 \\ 0 & 0 & \ddots & \vdots & \vdots \\ 0 & 0 & \dots & 2 & 0 \\ 0 & 0 & \dots & 0 & 1 \end{bmatrix}, \tag{48}$$

where r is chosen as 2.0 in this case. By defining R in this manner, the current control value is weighted H_p times heavier than the control value at the end of the prediction horizon. This prevents large controls from being chosen at the beginning of an update interval, even if significant error is present. The model update interval for the case shown in figure 2 is 1000 arc lengths, and the arc length step size, Δs, is 20. These parameters provide a good baseline from which to begin examining the performance of the model-predictive controller. Figures 5 and 6 show a typical controlled and uncontrolled trajectory with the model predictive control parameters set listed earlier.

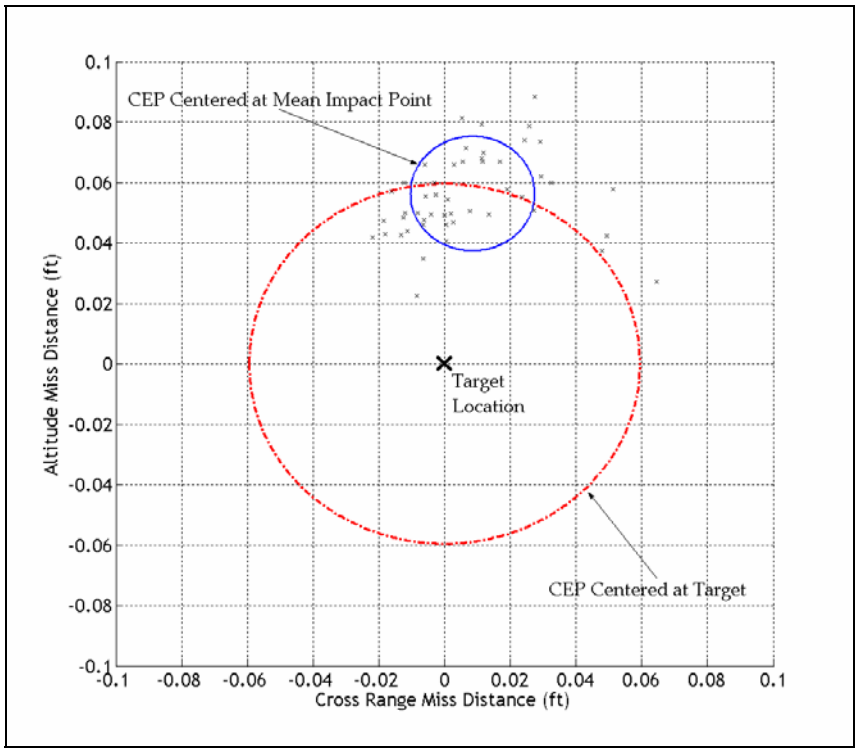

Figure 4. Controlled dispersion (CEP = 0.02 ft centered at mean impact point).

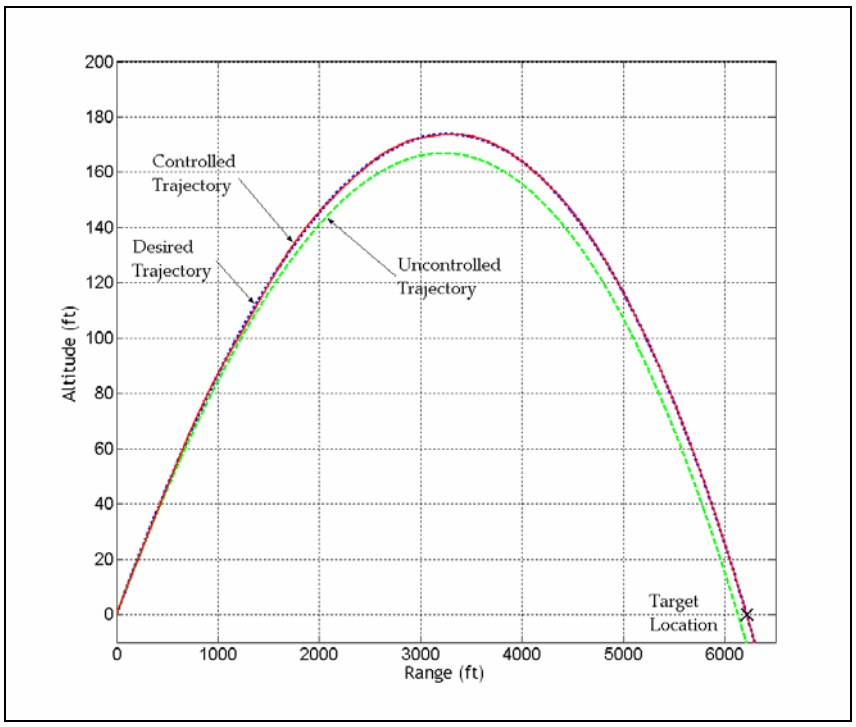

Figure 5. Typical altitude vs. range.

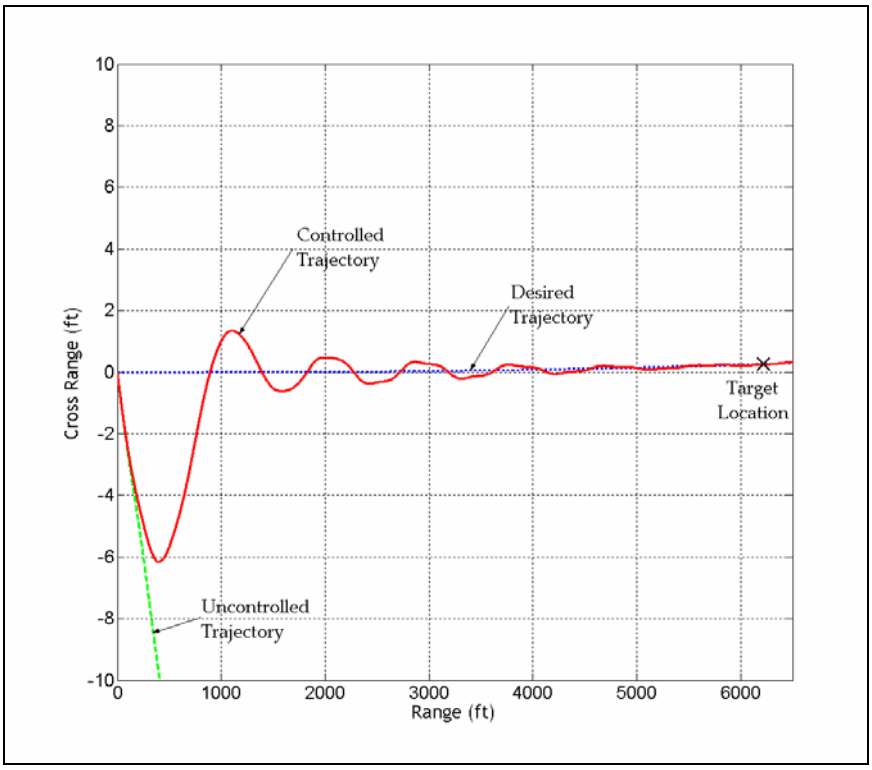

Figure 6. Typical cross range vs. range.

The model-predictive controller provides a very significant reduction in the CEP—from 106 ft, in the uncontrolled case, to 0.02 ft (or less than 1/4 in) with control applied. It should also be noted that the mean impact point is almost 0.06 ft, or ~0.75 in, above the target location. In the cross-range direction, however, the mean impact point is only 0.0085 ft away from the target. This bias error in the *z*-direction can be attributed directly to errors in the linear model used in the predictor. One of the primary assumptions upon which projectile linear theory is based is that the projectile maintains a small angle of attack. As the target is approached, the angle of attack of the projectile is forced to a small, nonzero number. Though it isn't necessarily in violation of the small angle of attack assumption, it is enough to cause a small deviation between the trajectory predicted with the linear model and that which is arrived at by integrating the full six-degree-of-freedom, nonlinear equations. This error is demonstrated by plotting the error between the validated, full six-degree-of-freedom, nonlinear trajectory, which is solved using a fixed step, 4th order Runge-Kutta method, and the linear theory trajectory solution. The linear solution is corrected to match the nonlinear solution every 1000 arc lengths to mimic flight control system feedback. The control input is set equal to zero in both cases and the initial conditions are set to match those used in creating the desired trajectory. Figure 7 shows the linear theory error as a function of arc length in the *x*, *y*, and *z* directions.

Note that the error is of the same order of magnitude near the end of the trajectory as the variation of the mean impact point in the CEP plot. It should also be noted that the error is

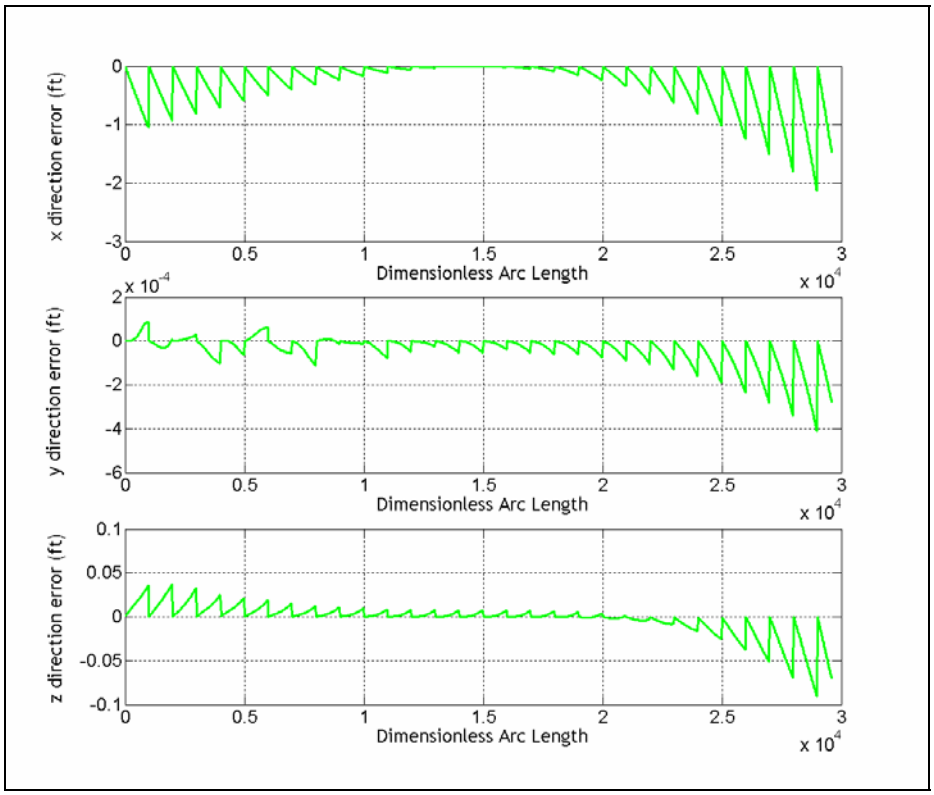

Figure 7. Error between linear and nonlinear trajectory solutions.

greatest at the beginning and end of the flight, where the trajectory is furthest from horizontal. At the midpoint of the trajectory, where the path of flight is nearly flat and the projectile angle of attack is nearly zero, the error in all three spatial directions also becomes very close to zero.

Figure 8 shows the required control inputs for the trajectory shown in figures 3 and 4. The magnitudes of the control inputs required to achieve the shown degree of tracking are attainable for a set of nose-mounted canards.

Great care must be taken when choosing the gain values, q and r, such that the control values, C_{Y0} and C_{Z0}, never exceed approximately one. Such large control inputs violate the small angle of attack assumption upon which the linearized model is based. As a result, the linear model no longer accurately approximates the true, nonlinear system, and the controller loses its ability to accurately predict future states. When the system is provided with state feedback from the IMU under these circumstances, there are very large errors and the controller subsequently attempts to choose a large control value to compensate. Within one to two update intervals, the error becomes large enough that control saturates.

Other applications of model predictive control, such as that discussed by Mei et al. (*2*), use an iterative scheme to set a maximum control input value. In the application being discussed, where speed of control computation is extremely critical, iteration is not practical. If the processor is occupied by an iterative routine while the projectile continues to fly downrange, control is lost.

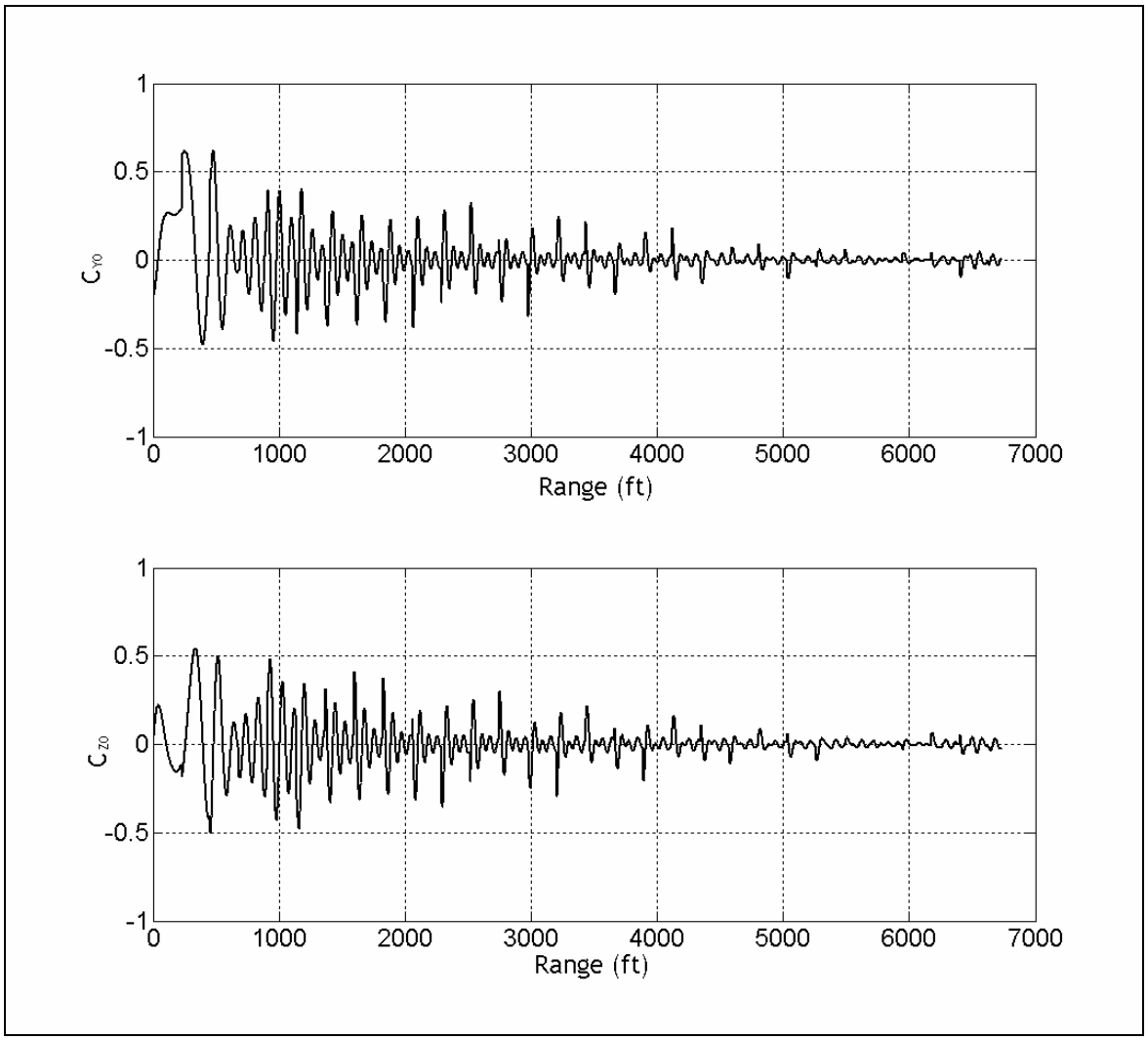

Figure 8. Required control inputs for a typical trajectory.

A second option is to simply clip the control values at the maximum allowable value. This, too, presents problems as future controls are calculated under the assumption that all previous controls were applied exactly as calculated. When this clipping scheme is attempted, the control begins oscillating rapidly between both allowable extremes, quickly resulting in instability.

The results discussed earlier assume perfect sensor feedback, which in reality can never be achieved. In practice, sensors possess error created by both bias and noise. These are modeled in the simulation by choosing normally-distributed random numbers with means of zero and standard deviations that are representative of commonly used IMU sensors. A bias value is randomly chosen for each sensor at the start of every flight simulation and retained throughout that particular simulation. In addition, a noise value is randomly chosen for each sensor every time feedback is implemented. Both the bias and noise value are added to the sensor readings at each update interval. The sensor bias and noise standard deviations used are summarized in

table 2. All subsequent results displayed in this report employ sensor bias and noise applied in this way.

Table 2. Sensor noise and bias values.

Sensor Function	Bias Standard Deviation	Noise Standard Deviation
x and *y* position (ft)	0.52	0.52
z position (ft)	1.18	1.18
x and *y* velocity (ft/s)	0.10	0.08
z velocity (ft/s)	0.16	0.13
roll, pitch, and yaw angles (deg)	0.3	0.3
roll, pitch, and yaw rates (deg/s)	0.05	0.01

Sensor noise and bias become the dominant sources of error when they are applied in this application. As the standard deviation of the sensor noise remains constant throughout the projectile flight, it no longer makes sense to define the error weighting matrix as a function of projectile range. Doing so, while keeping the value of q low enough to avoid violating the small angle of attack assumption near the end of the trajectory, unnecessarily limits the control action near the beginning of the trajectory. The error weighting matrix, Q, is instead defined simply as the identity matrix multiplied by the constant gain value, q.

Figure 9 shows dispersion results with sensor noise and bias applied. The prediction horizon, H_p, is again 50. The error gain, q, is set to 1. The control weighting matrix, R, is defined as shown in equation 48 with the gain value, r, equal to 0.2. The update interval is 1000 arc lengths and the arc length step size, Δs, is 20. As a direct result of the sensor uncertainty, the CEP radius is increased to 2.1 ft.

In figure 10, the effects of changing both the control gain, r, and the prediction horizon, H_p, are shown. The model update interval is held constant at 1000 arc lengths and the arc length step size is held constant at 20 arc lengths throughout all of the simulations shown in figure 10. In addition, the error weighting matrix, Q, is defined as the identity matrix with the error gain, q, equal to 1. The control weighting matrix, R, is again defined as shown in equation 48. The control gain, r, is varied from 0.025 to 10 with the prediction horizon held constant. The process is repeated four times with values of $H_P = 25$, $H_P = 50$, $H_P = 75$, and $H_P = 100$.

As the value of r is increased, additional weight is given to the value of the control in the cost function (equation 43). This in turn forces the magnitude of the chosen control values to be smaller, which provides less control authority. As would be expected, figure 10 shows that larger values of r lead to increased dispersion. However, there is a value of r below which the control values are allowed to be too large, leading to violation of the small angle of attack assumption and loss of control. This minimum value of r varies depending on the length of the prediction horizon. In figure 10, the lowest attempted values of r which resulted in a controllable trajectory are shown as the first data point for each series.

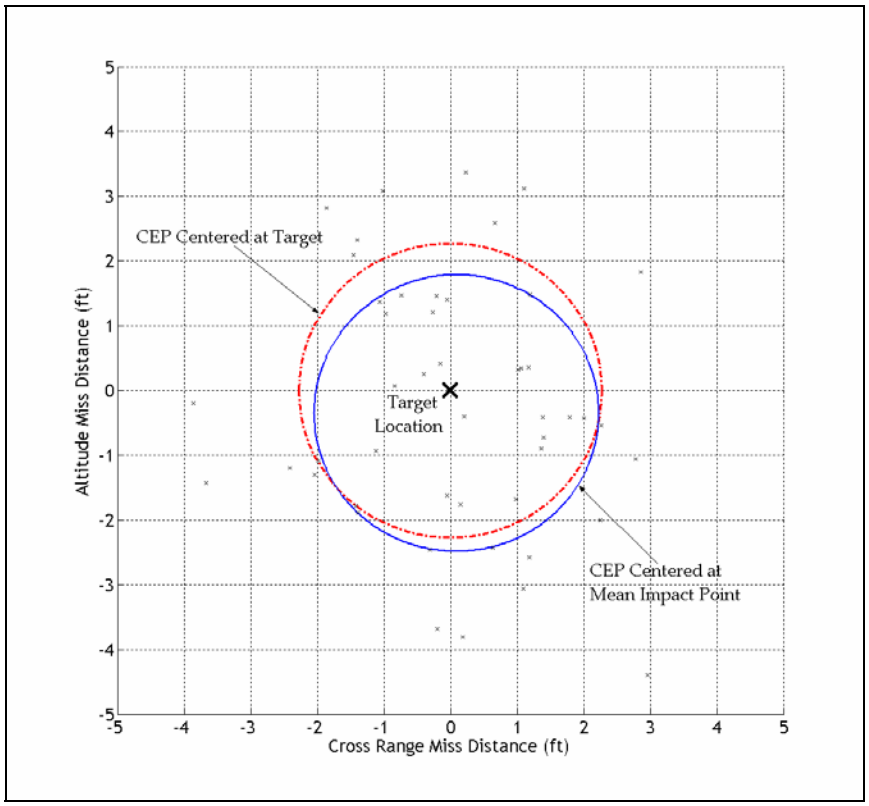

Figure 9. Controlled dispersion with sensor bias and noise applied (CEP = 2.1 ft centered at mean impact point).

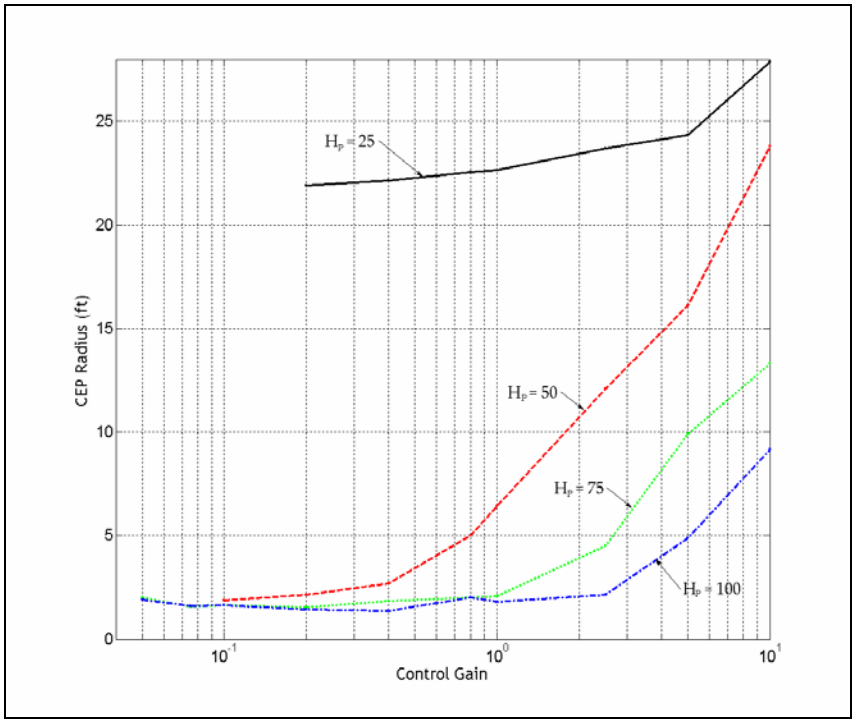

Figure 10. Controlled dispersion results as the control gain, r, is varied.

It is also apparent from figure 10 that, for a given value of *r*, there is a direct relationship between the length of the prediction horizon and the amount of impact point dispersion. Allowing the controller to take into account an increased number of the predicted states, as a longer prediction horizon does, leads to more intelligent control choices. It also significantly increases the amount of computation required at each update interval, necessitating a more expensive onboard processor.

A similar study was performed to investigate the effect of the length of the linear model update interval on the dispersion radius. The error weighting matrix, *Q*, is again the identity matrix with the error gain, *q*, set to one. The control weighting matrix, *R*, is defined as shown in equation 48 with the gain value, *r*, equal to 0.5. The arc length step size is again 20 arc lengths. The linear model update interval is varied from 100 to 2000 while holding the value of the prediction horizon constant. As before, the process is repeated four times with prediction horizon values of $H_P = 25$, $H_P = 50$, $H_P = 75$, and $H_P = 100$. The results are shown in figure 11.

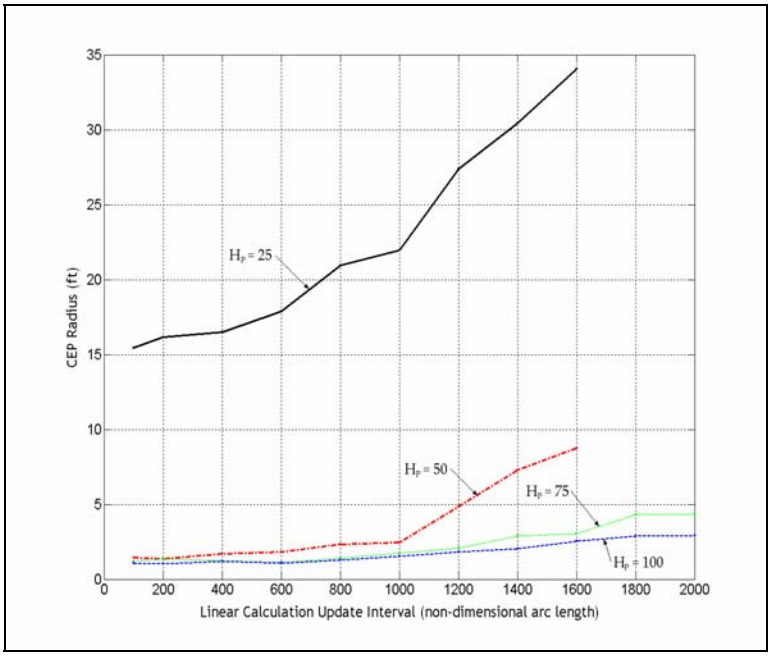

Figure 11. Controlled dispersion results as the linear model update interval is varied.

Longer linear model update intervals lead to an increase in dispersion. This increase becomes more apparent for update intervals greater than 1000 arc lengths. For prediction horizon lengths of 25 and 50 arc length steps, update intervals greater than 1600 arc lengths led to a loss of control. This results from the linearized model deviating too far from the true, nonlinear system. Upon update, the error becomes very large and a large control is chosen to compensate, which in turn violates the small angle of attack assumption and causes further error in the linear model. Reducing the error gain, *q*, or increasing the control gain, *r*, would prevent this scenario from

occurring. However, the tradeoff would be a reduction in control authority and an increase in dispersion.

The final study investigates the effects of the length of the step size, Δs, used by the controller to propagate the linear model forward. The prediction horizon is held constant at 50 steps and the error weighting matrix is the identity matrix with the gain, q, equal to one. The control weighting matrix is defined as shown in equation 48. Four values for the arc length step size ($\Delta s = 5$, $\Delta s = 10$, $\Delta s = 20$, and $\Delta s = 40$) are used while the control gain, r, is varied over the range which provided suitable control inputs for each step size. The results can be seen in figure 12.

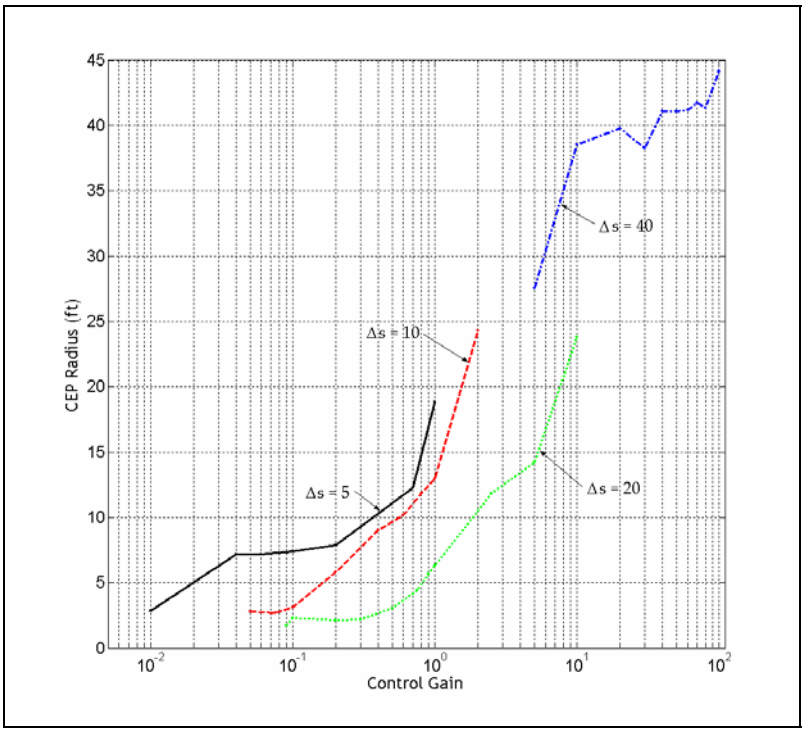

Figure 12. Controlled dispersion results as the arc length step size is varied.

As with any discrete, linear model, the length of the step size has no effect on the accuracy of the model itself. However, as evidenced by figure 12, the length of the arc length step size does have an effect on the overall accuracy of the controller. This results from an interplay between two competing effects. The prediction horizon length is measured in the number of steps into the future that are used in the calculation of the optimal control. Therefore, for a given prediction horizon length, increasing the arc length step size allows the predictor to take into account state values farther into the future. However, control values are only calculated at each step increment, with control values between calculation steps derived from linear interpolation. A large step size can therefore lead to a decrease in resolution of the controller. For arc length step sizes of 5, 10, and 20, these effects do little more than change the acceptable range of gains,

shifting the lines to the right on figure 12 for increasing values of Δs. However, at $\Delta s = 40$, the controller becomes unable to provide the necessary amount of oscillation and dispersion is increased dramatically.

6. Conclusions

This report develops a method for applying model predictive control, a proven and effective control technique, to a smart projectile application. The control law is shown to dramatically reduce the impact point dispersion caused by launch disturbances. The method uses full state feedback to create a linearized model of the projectile and quickly predict the future states of the system. These calculations can be performed by a relatively inexpensive onboard processor. As the predicted states depend on the states provided by the feedback loop, sensor accuracy is very important to the performance of the system and was shown here to be the limiting factor in dispersion reduction.

Considerable opportunities exist for the control system designer to tune the model-predictive controller based on the desired application. It was shown that the length of the prediction horizon has a considerable effect on the dispersion radius, with a longer prediction horizon leading to a decrease in dispersion. However, a longer prediction horizon increases the size of the matrices used in the control calculation, which subsequently necessitates an increase in the processing power required to perform control calculations in a sufficiently short period of time. Shorter linear model update intervals lead to a decrease in dispersion as well, but with a similar increase in the amount of onboard computation required. The length of the arc length step size was shown to have little effect on dispersion as long as it remained below 20 arc lengths. Control and error gains should be adjusted to allow sufficient control authority without violating any of the assumptions upon which linear theory is based. No iterative scheme is built into the controller to limit the size of the control inputs, so the control system designer should run a series of simulations prior to launching a projectile to ensure that the control and error gains are properly adjusted.

7. References

1. Camacho, E.; Bordons, C. *Model Predictive Control*; Springer-Verlag: London, 1999.
2. Mei, G.; Kareem, J.; Kantor, J. Model Predictive Control of Wind-Excited Building: Benchmark Study. *Journal of Engineering Mechanics* **2004**, *130* (4), 459–465.
3. Tsai, C.; Huang, C. Model Reference Adaptive Predictive Control for a Variable-Frequency Oil Cooling Machine. *IEEE Transactions on Industrial Electronics* **2004**, *51* (2), 2004.
4. Kvaternik, R.; Piatak, D.; Nixon, M.; Langston, C.; Singleton, J.; Bennett, R.; Brown, R. An Experimental Evaluation of Generalized Predictive Control for Tiltrotor Aeroelastic Stability Augmentation in Airplane Mode of Flight. *Journal of the American Helicopter Society* **2002**, *47* (3), 198–208.
5. Slegers, N.; Costello, M. Model Predictive Control of a Parafoil and Payload System. *Proceedings of the 2004 AIAA Atmospheric Flight Mechanics Conference*, Providence, RI, 2004; paper no. 2004-4822.
6. Burchett, B.; Costello, M. Model Predictive Lateral Pulsejet Control of an Atmospheric Rocket. *Journal of Guidance, Control, and Dynamics* **2002**, *25* (5), 860–867.
7. Costello, M.; Anderson, D. Effect of Internal Mass Unbalance on the Terminal Accuracy and Stability of a Projectile. *Proceedings of the 1996 AIAA Flight Mechanics Conference*, San Diego, CA, 1996.
8. Murphy, C. H. Symmetric Missile Dynamic Instabilities—A Survey. *18th AIAA Aerospace Sciences Meeting*, Pasadena, CA, 14–16 January 1980.
9. Hodapp, A. E. Effect of Mass Asymmetry on Ballistic Match of Projectiles. *Journal of Spacecraft and Rockets* **1976**, *13* (12), 757–760.
10. Weber, D. J. Simplified Method for Evaluating the Flight Stability of Liquid-Filled Projectiles. *Journal of Spacecraft and Rockets* **1994**, *31* (1), 130–134.
11. Murphy, C. H. Angular Motion of a Spinning Projectile With a Viscous Liquid Payload. *Journal of Guidance, Control, and Dynamics* **1983**, *6* (4), 280–286.
12. Cobb, K. K.; Whyte, R. H.; Laird, P. K. Effects of a Moving Components on the Motion of a 20-mm Projectile. *11th AIAA Aerodynamics Testing Conference*, Colorado Springs, CO, 18–20 March 1983; pp 94–103.
13. Hodapp, A. E. Passive Means for Stabilizing Projectiles With Partially Restrained Internal Members. *Journal of Guidance, Control, and Dynamics* **1989**, *12* (2), 135–139.

14. Soper, W. G. Projectile Instability Produced by Internal Friction. *AIAA Journal* **1978**, *16* (1), 8–11.

15. Costello, M.; Peterson, A. Linear Theory of a Dual-Spin Projectile in Atmospheric Flight. *Journal of Guidance, Control, and Dynamics* **2000**, *23* (5), 789–797.

16. Murphy, C. H. Instability of Controlled Projectiles in Ascending or Descending Flight. *Journal of Guidance and Control* **1981**, *4* (1), 66–69.

17. Cooper, G. Influence of Yaw Cards on the Yaw Growth of Spin Stabilized Projectiles. *Journal of Aircraft* **2001**, *38* (2), 266–270.

18. Guidos, B.; Cooper, G. Closed Form Solution of Finned Projectile Motion Subjected to a Simple In-Flight Lateral Impulse. *38th AIAA Aerospace Sciences Meeting and Exhibit*, Reno, NV, 2000; paper no. AIAA-2000-0767.

19. Burchett, B.; Peterson, A.; Costello, M. Prediction of Swerving Motion of a Dual-Spin Projectile With Lateral Pulsejets in Atmospheric Flight. *Mathematical and Computer Modeling* **2002**, *35* (1–2), 1–14.

20. Etkin, B. *Dynamics of Atmospheric Flight.* Wiley: New York, 1972.

21. McCoy, R. L. *Modern Exterior Ballistics*. Schiffer Military History: Atglen, PA, 1999.

22. Murphy, C. H. *Free Flight Motion of Symmetric Missiles*; BRL report no. 1216; U.S. Army Ballistic Research Laboratories: Aberdeen Proving Ground, MD, 1963.

23. Cooper, G.; Costello M. On the Response of Projectiles to Lateral Impulsive Loads. *Journal of Dynamic Systems, Measurement, and Control*, submitted for publication, 2004.

24. Ikonen, E.; Kaddour, N. *Advanced Process Identification and Control*. Marcel Dekker: New York.

List of Symbols, Abbreviations, and Acronyms

ρ:	Air density
C_{NA}:	Normal force aerodynamic coefficient
C_{MQ}:	Pitch rate damping moment aerodynamic coefficient
C_{X0}:	Aerodynamic drag coefficient in direction parallel to projectile motion
C_{Y0}, C_{Z0}:	Aerodynamic trim coefficients perpendicular to projectile axis of symmetry
C_{DD}:	Roll moment from fin cant
C_{YPA}:	Magnus force
C_{LP}:	Roll damping moment
D:	Projectile characteristic diameter
I_P, I_R:	Projectile precesional and rotational inertia
m :	Projectile mass
p, q, r :	Angular velocity vector components expressed in the body fixed reference frame
ψ, θ, ϕ:	Euler yaw, pitch, and roll angles
ΔSL:	Stationline distance from the projectile center of pressure location to the CG
ΔSL_m:	Stationline distance from the projectile Magnus force location to the CG
ΔSL_C:	Stationline distance from the control canard location to the CG
u, v, w :	Translation velocity components of the projectile center of mass resolved in the body fixed reference frame

x, y, z :	Position vector components of the projectile mass center expressed in the inertial reference frame
V :	Magnitude of the mass center velocity
L, M, N :	Total external applied moment on the rocket about the mass center expressed in the rocket reference frame
X, Y, Z :	Total external applied force on the rocket expressed in the rocket reference frame
H_p :	Prediction horizon used in model predictive controller
s :	Dimensionless arc length

NO. OF COPIES ORGANIZATION

1 (PDF ONLY) DEFENSE TECHNICAL INFORMATION CTR
DTIC OCA
8725 JOHN J KINGMAN RD
STE 0944
FORT BELVOIR VA 22060-6218

1 US ARMY RSRCH DEV & ENGRG CMD
SYSTEMS OF SYSTEMS INTEGRATION
AMSRD SS T
6000 6TH ST STE 100
FORT BELVOIR VA 22060-5608

1 INST FOR ADVNCD TCHNLGY
THE UNIV OF TEXAS
AT AUSTIN
3925 W BRAKER LN STE 400
AUSTIN TX 78759-5316

1 US MILITARY ACADEMY
MATH SCI CTR EXCELLENCE
MADN MATH
THAYER HALL
WEST POINT NY 10996-1786

1 DIRECTOR
US ARMY RESEARCH LAB
IMNE ALC IMS
2800 POWDER MILL RD
ADELPHI MD 20783-1197

3 DIRECTOR
US ARMY RESEARCH LAB
AMSRD ARL CI OK TL
2800 POWDER MILL RD
ADELPHI MD 20783-1197

3 DIRECTOR
US ARMY RESEARCH LAB
AMSRD ARL CS IS T
2800 POWDER MILL RD
ADELPHI MD 20783-1197

NO. OF COPIES ORGANIZATION

ABERDEEN PROVING GROUND

1 DIR USARL
AMSRD ARL CI OK TP (BLDG 4600)

NO. OF COPIES	ORGANIZATION
3	AIR FORCE RSRCH LAB MUNITIONS DIR AFRL/MNAV G ABATE 101 W EGLIN BLVD STE 219 EGLIN AFB FL 32542
1	CDR WL/MNMF D MABRY 101 W EGLIN BLVD STE 219 EGLIN AFB FL 32542-6810
20	OREGON STATE UNIV DEPT OF MECHL ENGRG M COSTELLO CORVALLIS OR 97331
4	CDR US ARMY ARDEC AMSTA AR CCH J DELORENZO S MUSALI R SAYER P DONADIO PICATINNY ARESENAL NJ 07806-5000
7	CDR US ARMY TANK MAIN ARMAMENT SYSTEM AMCPM TMA D GUZIEWICZ R DARCEY C KIMKER R JOINSON E KOPOAC T LOUZIERIO C LEVECHIA PICATINNY ARESENAL NJ 07806-5000
1	CDR USA YUMA PROV GRND STEYT MTW YUMA AZ 85365-9103
1	DIR BENET LABORATORIES SMCWV QAR T MCCLOSKEY WATERVLIET NY 12189-5000

NO. OF COPIES	ORGANIZATION
10	CDR US ARMY TACOM AMCPEO HFM AMCPEO HFM F AMCPEO HFM C AMCPM ABMS AMCPM BLOCKIII AMSTA CF AMSTA Z AMSTA ZD AMCPM ABMS S W DR PATTISON A HAVERILLA WARREN MI 48397-5000
1	CDR USAOTEA CSTE CCA DR RUSSELL ALEXANDRIA VA 22302-1458
2	DIR US ARMY ARMOR CTR & SCHL ATSB WP ORSA A POMEY ATSB CDC FT KNOX KY 40121
1	CDR US ARMY AMCCOM AMSMC ASR A MR CRAWFORD ROCK ISLAND IL 61299-6000
2	PROGRAM MANAGER GROUND WEAPONS MCRDAC LTC VARELA CBGT QUANTICO VA 22134-5000
4	COMMANDER US ARMY TRADOC ATCD T ATCD TT ATTE ZC ATTG Y FT MONROE VA 23651-5000
1	NAWC F PICKETT CODE C2774 CLPL BLDG 1031 CHINA LAKE CA 93555

NO. OF COPIES ORGANIZATION

1 NAVAL ORDNANCE STATION
ADVNCD SYS TCHNLGY BRNCH
D HOLMES
CODE 2011
LOUISVILLE KY 40214-5001

1 NAVAL SURFACE WARFARE CTR
F G MOORE
DAHLGREN DIVISION
CODE G04
DAHLGREN VA 22448-5000

1 US MILITARY ACADEMY
MATH SCI CTR OF EXCELLENCE
DEPT OF MATHEMATICAL SCI
MDN A MAJ DON ENGEN
THAYER HALL
WEST POINT NY 10996-1786

3 DIR
SNL
A HODAPP
W OBERKAMPF
F BLOTTNER
DIVISION 1631
ALBUQUERQUE NM 87185

1 ALLIANT TECH SYS
TCAAP
R BECKER
BLDG 104
ARDEN HILLS MN 55112

1 ALLIANT TECH SYS
C CANDLAND
4700 NATHAN LN
PLYMOUTH MN 55442

1 UNITED DEFENSE LP
R BURETTA
CODE M170
4800 E RIVER RD
MINNEAPOLIS MN 55421

3 DIR USARL
AMSRL SE RM
H WALLACE
AMSRL SS SM
J EIKE
A LADAS
2800 POWDER MILL RD
ADELPHI MD 20783-1145

NO. OF COPIES ORGANIZATION

2 CDR USARDEC
AMSTA FSP A
S DEFEO
R SICIGNANO
PICATINNY ARSENAL NJ
07806-5000

2 CDR USARDEC
AMSTA AR CCH A
M PALATHINGAL
R CARR
PICATINNY ARSENAL NJ
07806-5000

5 TACOM ARDEC
AMSTA AR FSA
K CHIEFA
AMSTA AR FS
A WARNASCH
AMSTA AR FSF
W RYBA
AMSTA AR FSP
S PEARCY
J HEDDERICH
PICATINNY ARSENAL NJ
07806-5000

5 CDR US ARMY MICOM
AMSMI RD
P JACOBS
P RUFFIN
AMSMI RD MG GA
C LEWIS
AMSMI RD MG NC
C ROBERTS
AMSMI RD ST GD
D DAVIS
RSA AL 35898-5247

3 CDR US ARMY AVN TRP CMD
DIRECTORATE FOR ENGINEERING
AMSATR ESW
M MAMOUD
M JOHNSON
J OBERMARK
RSA AL 35898-5247

1 DIR US ARMY RTTC
STERT TE F TD
R EPPS
BLDG 7855
REDSTONE ARSENAL AL
38598-8052

NO. OF COPIES ORGANIZATION

2 STRICOM
AMFTI EL
D SCHNEIDER
R COLANGELO
12350 RESEARCH PKWY
ORLANDO FL 32826-3276

1 CDR OFFICE OF NAVAL RES
J GOLDWASSER CODE 333
800 N QUINCY ST RM 507
ARLINGTON VA 22217-5660

1 CDR US ARMY RES OFFICE
AMXRO RT IP TECH LIB
PO BOX 12211
RESEARCH TRIANGLE PARK NJ
27709-2211

4 CDR US ARMY AVN TRP CMD
AVIATION APPLIED TECH DIR
AMSATR TI
R BARLOW
E BERCHER
T CONDON
B TENNEY
FT EUSTIS VA 23604-5577

3 CDR NAWC
WEAPONS DIV
CODE 543400D
S MEYERS
CODE C2744
T MUNSINGER
CODE C3904
D SCOFIELD
CHINA LAKE CA 93555-6100

1 CDR NSWC
CRANE DIVISION
CODE 4024
J SKOMP
300 HIGHWAY 361
CRANE IN 47522-5000

1 CDR NSWC
DAHLGREN DIV
CODE 40D
J BLANKENSHIP
6703 WEST HWY 98
PANAMA CITY FL 32407-7001

NO. OF COPIES ORGANIZATION

2 CDR NSWC
J FRAYSEE
D HAGEN
17320 DAHLGREN RD
DAHLGREN VA 22448-5000

5 CDR NSWC
INDIAN HEAD DIV
D GARVICK CODE 40D
L FAN CODE 4110C
V CARLSON CODE 4120
H LAST CODE 4140E
T GRIFFIN CODE 450D
101 STRAUSS AVE
INDIAN HEAD MD 20640-5000

1 CDR NSWC
INDIAN HEAD DIV
LIBRARY CODE 8530
BLDG 299
101 STRAUSS AVE
INDIAN HEAD MD 20640

2 US MILITARY ACADEMY
MATH SCI CTR OF EXCELLENCE
DEPT OF MATHEMATICAL SCI
MDN A
MAJ D ENGEN
R MARCHAND
THAYER HALL
WEST POINT NY 10996-1786

3 CDR US ARMY YUMA PG
STEYP MT AT A
A HOOPER
STEYP MT EA
YUMA AZ 85365-9110

6 CDR NSWC
INDIAN HEAD DIV
CODE 570D J BOKSER
CODE 5710 L EAGLES
J FERSUSON
CODE 57 C PARIS
CODE 5710G S KIM
CODE 5710E S JAGO
101 STRAUSS AVE ELY BLDG
INDIAN HEAD MD 20640-5035

1 MICHIGAN STATE UNIV
B KIM
2120 ENGINEERING BLDG
EAST LANSING MI 48824-1226

NO. OF COPIES ORGANIZATION

2 INDUSTRIAL OPERATION CMD
AMFIO PM RO
W MCKELVIN
MAJ BATEMAN
ROCK ISLAND IL 61299-6000

3 PROGRAM EXECUTIVE OFFICER
TACTICAL AIRCRAFT PROGRAMS
PMA 242 1
MAJ KIRBY R242
PMA 242 33
R KEISER (2 CPS)
1421 JEFFERSON DAVIS HWY
ARLINGTON VA 22243-1276

3 ARROW TECH ASSOCIATES INC
R WHYTE
A HATHAWAY
H STEINHOFF
1233 SHELBOURNE RD STE D8
SOUTH BURLINGTON VT 05403

3 US ARMY AVIATION CTR
DIR OF COMBAT DEV
ATZQ CDM C
B NELSON
ATZQ CDC C
T HUNDLEY
ATZQ CD
G HARRISON
FORT RUCKER AL 36362

1 US ARMY CORPS OF ENGINEERS
CEERD ZA T
W MORRISON
7701 TELEGRAPH RD
KINGMAN BLDG RM 322
ALEXANDRIA VA 22315

1 DIRCTRT OF TRAINING, DOCTRINE,
AND COMBAT DEV
ATZK TDD ORSA
A POMEY
RM 202 HARRIS HALL
BLDG 2368 OLD IRONSIDES AVE
FORT KNOX KY 40121-5000

NO. OF COPIES ORGANIZATION

ABERDEEN PROVING GROUND

3 CDR
USA ARDEC
AMSTA AR FSF T
R LIESKE
J WHITESIDE
J MATTS
BLDG 120

1 CDR
USA TECOM
AMSTE CT
T J SCHNELL
RYAN BLDG

3 CDR
USA AMSAA
AMXSY EV
G CASTLEBURY
R MIRABELLE
AMXSY EF
S MCKEY

43 DIR USARL
AMSRD ARL WM
T ROSENBERGER
AMSRD ARL WM BA
W HORST JR
W CIEPELLA
F BRANDON
T BROWN (5 CPS)
L BURKE
J CONDON
B DAVIS
T HARKINS (5 CPS)
D HEPNER
V LEITZKE
M HOLLIS
A THOMPSON
G BROWN
AMSRD ARL WM BB
B HAUG
AMSRD ARL WM BC
P PLOSTINS (4 CPS)
G COOPER
B GUIDOS
J SAHU
M BUNDY
D LYON
AMSRD ARL WM BC
J BENDER
J GARNER
S WILKERSON

NO. OF
COPIES ORGANIZATION

W DRYSDALE
R COATES
A MIKHAL
J WALL
AMSRD ARL WM BD
B FORCH
AMSRD ARL WM BE
M SCHMIDT
AMSRD ARL WM BF
AMSRD ARL WM BR
C SHOEMAKER
J BORNSTEIN

INTENTIONALLY LEFT BLANK.